12-2007

The Effect of a Skyrme Interaction on Nucleon Induced Reactions

Yingfa Zhang
Western Michigan University

THE EFFECT OF A SKYRME INTERACTION ON NUCLEON INDUCED REACTIONS

by

Yingfa Zhang

A Thesis
Submitted to the
Faculty of The Graduate College
in partial fulfillment of the
requirements for the
Degree of Master of Arts
Department of Physics

Western Michigan University
Kalamazoo, Michigan
December 2007

THE EFFECT OF A SKYRME INTERACTION ON NUCLEON INDUCED REACTIONS

Yingfa Zhang, M.A.

Western Michigan University, 2007

The main goal of this Master thesis is the theoretical study of the interaction between a nucleon and a nucleus. This is a fundamental method to study the structure and dynamics of nuclear systems. This thesis concentrates on the study of nucleon scattering on light nuclei, ^{6}Li, ^{7}Li and ^{14}N, with the effective interaction M3Y and its modification by adding a Skyrme force. This is the first time the Skyrme interaction has been employed in scattering calculations. From a comparison of the measured differential cross section $\sigma(\theta)$ and the analyzing power $A_y(\theta)$ for ^{6}Li and ^{7}Li with the corresponding calculations, we can conclude that inclusion of the Skyrme interaction reduces agreement with the experimental data in lower proton energies, but improves agreement at higher proton energies.

TABLE OF CONTENTS

LIST OF FIGURES

List of Figures—continued

CHAPTER I

INTRODUCTION

The interaction between a nucleon and a nucleus is a fundamental method to study the structure and dynamics of nuclear systems. Elastic, inelastic, and charge-exchange reactions play a fundamental role for understanding the nucleon-nucleon (NN) interaction. Comparisons of differential cross section $\sigma(\theta)$ and the analyzing power $A_y(\theta)$ measurements with the corresponding calculations can provide information on the components of the effective NN interaction.

This thesis concentrates on the study of nucleon scattering on light nuclei with the effective interaction M3Y [1] and the modification to this interaction at beginning of the p-shell [2]. The most important modification is the addition of a Skyrme force [3] which is traditionally used in structure calculations. This is the first time the Skyrme interaction has been employed in scattering calculations.

Previous investigations of realistic effective interactions have employed the distorted wave Born approximation (DWBA). In this thesis, the recoil corrected continuum shell model (RCCSM) [2, 4-5] is used to calculate the cross sections and analyzing powers. The RCCSM does not rely on optical potentials, but is used to solve the dynamical scattering equations generated from the basic Hamiltonian.

In chapter II the different effective forces are described. The basis for these interactions is the M3Y interaction. The M3Y interaction has been shown to be the near perfect effective interaction for the RCCSM in the $A = 4$ systems [6] and it has also been shown that the M3Y interaction gives a reasonable description of medium energy nucleon scattering in the lower part of the p-shell [2, 7-8]. However, for

structure calculations and very low energy reactions in the p-shell, in order to obtain the correct thresholds, it is necessary to add a repulsive Skyrme interaction to M3Y. This work determines how the Skyrme interaction affects those medium energy elastic and inelastic scattering of nucleons.

The results are shown for elastic scattering and inelastic scattering with different proton energies, which includes the $^{6}Li(p,p)$ reaction at $E_p = 49.75\ MeV$; $^{7}Li(p,n)^{7}Be$ reaction at $E_p = 18.9\ MeV$, $E_p = 26\ MeV$ and $E_p = 45\ MeV$; $^{7}Li(p,p')^{7}Li$ reaction at $E_p = 24.4\ MeV$ and $E_p = 49.8\ MeV$; and $^{14}N(p,p)^{14}N$ reaction at $E_p = 30\ MeV$. Calculations are performed with the three different effective interactions presented in chapter II. It is concluded that inclusion of the Skyrme interaction reduces agreement with the experimental data in lower proton energies, but improves agreement at higher proton energies.

CHAPTER II

THEORY

The M3Y Interaction

The Michigan three Yukawa (M3Y) effective nucleon-nucleon interactions were initially developed for DWA calculations. The interaction is parameterized as the sum of three Yukawas potentials. It is based on the G-matrix elements and supplemented by available emperical shell model matrix elements. This effective NN interaction takes in the following form:

$$V_c = \sum V_i Y(r_{12}/R_i), \text{ central}$$

$$V_{so} = \sum V_i Y(r_{12}/R_i)\vec{L}\bullet\vec{S}, \text{ Spin-Orbit}$$

$$V_t = \sum V_i r_{12}^2 Y(r_{12}/R_i)S_{12}, \text{ tensor}$$

or the regularized one-pion exchange potential (OPEP)

$$V = V_3[Z(r_{12}/R_{\max}) - (R_{\max}/R_2)^3 Z(r_{12}/R_2)]S_{12}$$

In these equations, the Yukawas potentials, $Y(X) = e^{-X}/X$, $Z(X) = (1+3/X+3/X^2)Y(X)$, S_{12} is the tensor operator, and $\vec{\mathbf{L}}\bullet\vec{\mathbf{S}}$ is the spin-orbit operator. Typical relative coordinate matrix elements are

$$<^3S_1 \mid S_{12} \mid ^3D_1> = \sqrt{8}, \quad <^3P_0 \mid \mathbf{L}\bullet\mathbf{S} \mid ^3P_0> = -2.$$

The ranges of the M3Y forces were chosen to ensure a long-range tail of the one-pion exchange potential as well as a short range repulsive part simulating the exchange of heavier mesons. V_i is determined by fitting to matrix elements.

Three approaches were employed in [1] to develop the realistic interactions:

(1). The scattering operator given by the Fourier transform of the separated

Hamada - Johnston (HJ) potential [9].

(2). G-matrix elements of the Reid potential [10] in an oscillator basis.

(3). The empirical oscillator matrix elements of Elliott [11].

1. Fit to small momentum components of the HJ interaction.

The separation distance for the potential is determined for the singlet-even (SE), triplet even (TE) and tensor-even (TNE) channels to be 1.05, 1.07 and 1.07fm respectively. The result is that SE is in good agreement with the corresponding numbers obtained from Reid and Elliott; however, for the TE and TNE, the HJ values are smaller compared to Reid.

2. Fit to Reid g-matrix elements

For this method one fits the harmonic oscillator matrix elements of the Yukawa sum to a partial set of G-matrix elements. The G-matrix elements of the $^1S_0$ and $^1P_1$ are corresponding to SE and singlet-odd (SO), and the coupled $^3S_1$ and $^3D_1$ are corresponding to TE and TNE. The tensor odd and spin-orbit components can be obtained from the following equation:

$$V(TO) = V(^3P_0) + 2V(LSO) + 4V(TNO)$$

$$V(TNO) = (-5/72)[2V(^3P_0) - 3V(^3P_1) + V(^3P_2)]$$

$$V(LSE) = (-1/60)[9V(^3D_1) + 5V(^3D_2) - 14V(^3D_3)]$$

$$V(LSO) = (-1/12)[2V(^3P_0) + 3V(^3P_1) - 5V(^3P_2)]$$

3. Fit to Elliot empirical matrix elements

The same fitting process applied to the Reid g-matrix elements is applied to the Elliot empirical matrix elements. The combinations of matrix elements used in this work are those given on page 412 of [1] and will be referred to as M3Y in the following.

The Skyrme Interaction

The Skyrme interaction was introduced into nuclear physics more than 50 years ago. Vautherin and Brink [12] revived an earlier idea of Skyrme for a parameterized interaction, which fit some ground state properties, binding energies, and densities of nuclear matter and a few light closed-shell nuclei.

Skyrme originally considered a two and three body potential

$$T = \sum\sum t_{ij}(for, i < j) + \sum\sum\sum t_{ijk}(for, i < j < k)$$

The first term is two-body, and the second term is for the three-body. This three-body term weakens the interaction in the nuclear interior.

For the two-body term, it can be expressed as:

$$t_{12} = \delta(\mathbf{r}_1 - \mathbf{r}_2)t(\mathbf{K}', \mathbf{K});$$

where $\mathbf{K}$ is the operator corresponding to the relative wave-number,

$$\mathbf{K} = (1/2)i(\nabla_1 - \nabla_2).$$

This two-body term will be replaced by the realistic effective interaction M3Y.

The three-body term as originally given by Skyrme can be written as:

$$t_{123} = \delta(\mathbf{r}_1 - \mathbf{r}_2)\delta(\mathbf{r}_3 - \mathbf{r}_1)t_3;$$

where t_3 is greater than zero. It was shown by Vautherin that this interaction can be replaced with a two-body interaction with the density dependence. This can be seen by the following argument.

Consider a typical p-shell matrix element

$$m = \int\phi_1^*(\mathbf{r}_1)\phi_2^*(\mathbf{r}_2)\phi_3^*(\mathbf{r}_3)t_3\delta(\mathbf{r}_1 - \mathbf{r}_2)\delta(\mathbf{r}_2 - \mathbf{r}_3)\phi_1(\mathbf{r}_1)\phi_2(\mathbf{r}_2)\phi_3(\mathbf{r}_3)d^3r_1d^3r_2d^3r_3$$

$$= \int[\phi_1^*(\mathbf{r}_2)\phi_1(\mathbf{r}_2)]\phi_2^*(\mathbf{r}_2)\phi_3^*(\mathbf{r}_3)t_3\delta(\mathbf{r}_2 - \mathbf{r}_3)\phi_2(\mathbf{r}_2)\phi_3(\mathbf{r}_3)d^3r_2d^3r_3 \qquad (1)$$

The matrix element is zero unless $\mathbf{r}_2 = \mathbf{r}_3$, so one may replace $\phi_1^*(\mathbf{r}_2)\phi_1(\mathbf{r}_2)$ by $\phi_1^*(\frac{\mathbf{r}_2 + \mathbf{r}_3}{2})\phi_1(\frac{\mathbf{r}_2 + \mathbf{r}_3}{2})$. This term now depends on the density at the center of mass of the two particles 2 and 3. The matrix element is now

$$m = \int \rho(\mathbf{R}_{23}) \phi_2^*(\mathbf{r}_2) \phi_3^*(\mathbf{r}_3) t_3 \delta(\mathbf{r}_2 - \mathbf{r}_3) \phi_2(\mathbf{r}_2) \phi_3(\mathbf{r}_3) d^3 r_2 d^3 r_3 \qquad (2)$$

The matrix looks like a two-body, density dependent matrix element, stronger (more repulsive) on the nuclear interior and weaker (less repulsive) on the surface. The form of equation (2) is preferable in structure calculations because it is a two-body matrix element and easy to calculate. The form in equation (1) is much more difficult to calculate, however it must be used in the RCCSM because it is translational invariant whereas the center of mass vector in equation (2) depends on the choice of origin.

The RCCSM calculation for the additional three-body force can be demonstrated in Fig. 1. The first diagram shows that three valence particles can interact with each other outside of the closed shell, and two valence particles interacting with one core nucleon can be described in second diagram. Finally the third graph describes the interaction between one valence nucleon and two core nucleons.

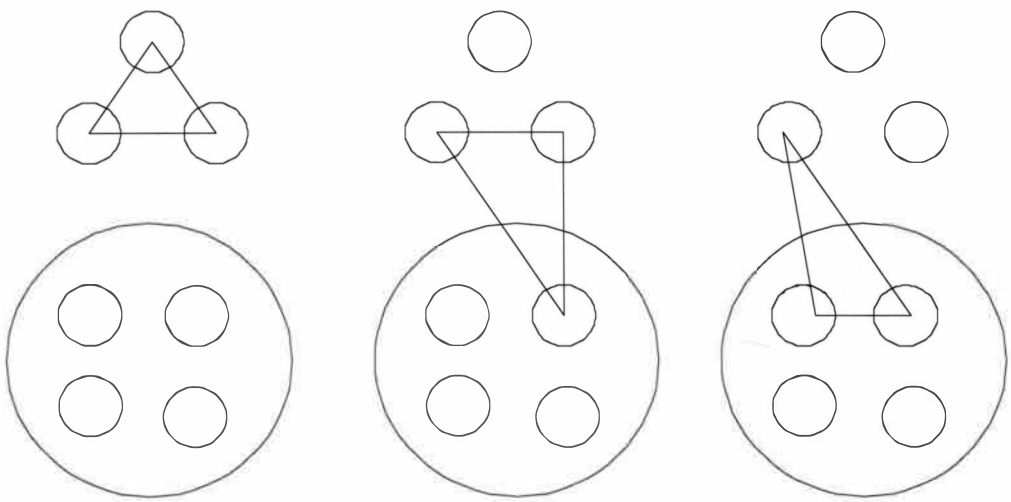

Figure 1: Three-Body Force.

This third diagram corresponds to the Skyrme contribution to the single particle energy. Since the formula expressions for the three body interaction for a specific p-shell nucleus are complicated and lengthy [5, 8], it will not be shown here, however, the basic three-body matrix element is given by:

$$< j_1(j_2 j_3)^{J_{23}}(J) \mid v \mid j_1'(j_2' j_3')^{J_{23}'}(J) >_A = <1> - <2> - <3> - <4> + <5>$$

$$+ <6> \tag{3}$$

$$<1> = < j_1(j_2 j_3)^{J_{23}}(J) \mid v \mid j_1'(j_2' j_3')^{J_{23}}(J) >_D \delta_{\tau_1\tau_1'}\delta_{\tau_2\tau_2'}\delta_{\tau_3\tau_3'} \tag{4}$$

$$<2> = (-1)^{j_1'+j_2'+j_3'+J} \hat{J}_{23}' \sum_{J_x} \hat{J}_x W(j_3' j_2' j_1'; J_{23}' J_x) < j_1(j_2 j_3)^{J_{23}}(J) \mid v \mid j_3'(j_2' j_1')^{J_x'}$$

$$(J) >_A \times \delta_{\tau_1\tau_3'}\delta_{\tau_2\tau_2'}\delta_{\tau_3\tau_1'} \tag{5}$$

$$<3> = (-1)^{j_3'+J+J_{23}'} \hat{J}_{23}' \sum_{J_x} (-1)^{J_x} \hat{J}_x W(j_2' j_3' J j_1'; J_{23}' J_x) < j_1(j_2 j_3)^{J_{23}}(J) \mid v \mid j_2'(j_1' j_3')^{J_x'}$$

$$(J) >_A \times \delta_{\tau_1\tau_2'}\delta_{\tau_2\tau_1'}\delta_{\tau_3\tau_3'} \tag{6}$$

$$<4> = (-1)^{j_2'+j_3'-J_{23}'} < j_1(j_2 j_3)^{J_{23}}(J) \mid v \mid j_1'(j_3' j_2')^{J_{23}'}(J) >_A \delta_{\tau_1\tau_1'}\delta_{\tau_2\tau_3'}\delta_{\tau_3\tau_2'} \tag{7}$$

$$<5> = (-1)^{j_3'+J+1} \hat{J}_{23}' \sum_{J_x} (-1)^{J_x} \hat{J}_x W(j_3' j_2' J j_1'; J_{23}' J_x) < j_1(j_2 j_3)^{J_{23}}(J) \mid v \mid j_3'(j_1' j_2')^{J_{23}'}$$

$$(J) >_A \times \delta_{\tau_1\tau_3'}\delta_{\tau_2\tau_1'}\delta_{\tau_3\tau_2'} \tag{8}$$

$$<6> = (-1)^{J_{23}'-j_1'+J} \hat{J}_{23}' \sum_{J_x} \hat{J}_x W(j_2' j_3' J j_1'; J_{23}' J_x) < j_1(j_2 j_3)^{J_{23}}(J) \mid v \mid j_2'(j_3' j_1')^{J_{23}'}$$

$$(J) >_A \times \delta_{\tau_1\tau_2'}\delta_{\tau_2\tau_3'}\delta_{\tau_3\tau_1'} \tag{9}$$

Where index D is the direct matrix element, and for (p,n), $\tau_i = (-1/2,+1/2)$. For the Skyrme interaction the six terms reduce to a radial integral and Clebsh-Gordan coefficients as given in the Appendix II. For an isospin coupled matrix, the Kronecker deltas in equations (4)-(9), $\delta_{\tau_1\tau_1'}\delta_{\tau_2\tau_2'}\delta_{\tau_3\tau_3'}$, $\delta_{\tau_1\tau_3'}\delta_{\tau_2\tau_2'}\delta_{\tau_3\tau_1'}$, $\delta_{\tau_1\tau_2'}\delta_{\tau_2\tau_1'}\delta_{\tau_3\tau_3'}$, $\delta_{\tau_1\tau_{11}}\delta_{\tau_2\tau_3'}\delta_{\tau_3\tau_2'}$, $\delta_{\tau_1\tau_3'}\delta_{\tau_2\tau_1'}\delta_{\tau_3\tau_2'}$, $\delta_{\tau_1\tau_2'}\delta_{\tau_2\tau_3'}\delta_{\tau_3\tau_1'}$ will be replaced as:

$\delta_{T_{23}T_{23}'}$,

$(-1)^{1/2+T} \hat{T}_{23}' \hat{T}_{23} W(1/2,1/2,T,1/2;\hat{T}_{23}' T_{23})$,

$(-1)^{1/2+T+T_{23}'-T_{23}} \hat{T}_{23}' \hat{T}_{23} W(1/2,1/2,T,1/2;\hat{T}_{23}' T_{23})$,

$(-1)^{1-T_{23}'}\delta_{T_{23}T_{23}'}$,

$(-1)^{T-T_{23}-1/2}\hat{T}_{23}'\hat{T}_{23}W(1/2,1/2,T,1/2;\hat{T}_{23}'T_{23}$,

$(-1)^{T+T_{23}-1/2}\hat{T}_{23}'\hat{T}_{23}W(1/2,1/2,T,1/2;\hat{T}_{23}'T_{23})$.

Description of RCCSM

The continuum shell model is used to investigate nuclear reactions involving one particle in the continuum. It was originally introduced by Fano [13] and placed in a formal context by Block [14]. This model is employed in many different reactions. It traverses the boundary between nuclear many body structure and nuclear reactions. Initial formulations of a continuum shell model were not useful for reactions involving light systems. The problem was the use of coordinates measured from a fixed point in space, and hence the continuum wave functions contained spurious components. In order to solve this problem, Philpott [15] formulated a new model, the recoil corrected continuum shell model (RCCSM), which is translationally invariant. Corrections are applied for target recoil. In addition to the Coulomb force, the effective NN interaction included central, spin-orbit, and tensor components.

One of the most successful applications of the RCCSM model is the 1p1h orbital [6]. One example is the reaction $^{12}C(\pi^{\pm},\pi^{\pm})^{12}C(4^{-})$. In $^{12}C(\pi^{\pm},\pi^{\pm})^{12}C(4^{-})$, the two 4^{-} states are almost completely isospin mixed, and the cross sections are different for $^{12}C(\pi^{+},\pi^{+})^{12}C(4^{-})$ and $^{12}C(\pi^{-},\pi^{-})^{12}C(4^{-})$ reactions. A modification of the M3Y interaction in the 1p-1h model could explain this result. It is because both 4^{-} states lie above the particle threshold and have a continuum contribution the level energies and to the mixing matrix elements. Many examples of the success of the 1p1h approximation were in the $A=4$ composite system. For ^{4}He, the M3Y interaction was shown to be an almost perfect effective interaction for the RCCSM with continuum nucleon energy less than $60\ MeV$. For

example, in ^{4}He, the small form factor for (e,e') for the 0^+ state at $E_x = 20.5\ MeV$ was explained by the RCCSM continuum wave functions [5]. Another application of RCCSM was in the structure of hypernuclei [6]. Because the hyperon mass differs from that of the proton and neutron , conventional shell model techniques of removing spurious center of mass excitations do not work.

The p-shell is another example for using RCCSM model. The p-shell codes include all p-shell states of the A-particle system and states where a nucleon is coupled to the desired core states of the A-1 systems. Calculations have been performed for the $A = 7$, 8, and 15 composite systems. In the $A = 8$ system, it is important to extrapolate measurements and calculations of $^7Be(p,\gamma)^8B$ to zero energy because the center of the Gamow window in $^7Be(p,\gamma)^8B$ is near $20\,KeV$, while the data are limited to above $100\,KeV$. One needs an accurate prediction for the 8B spectra above the threshold, and this is because resonances can contribute to low energy capture. However, in order to correct the thresholds, it is necessary to add a repulsive Skyrme interaction to M3Y, because without this interaction, low-lying states are overbound. This work determines how the three-body Skyrme interaction affects those medium energy elastic and inelastic scattering of nucleons.

The RCCSM employs the R-matrix formalism for calculating the cross section and the analyzing power. The dynamical R-matrix equations (Robson) are solved by the transformation procedure of Philpott [16]. Then the standard equations for the cross section and analyzing power given in Lane and Thomas [17] are solved.

CHAPTER III

COMPUTATIONS

As mentioned in previous chapter, RCCSM employed an R-matrix to calculate the cross section and the analyzing power. The procedure can be explained following the flow diagram below.

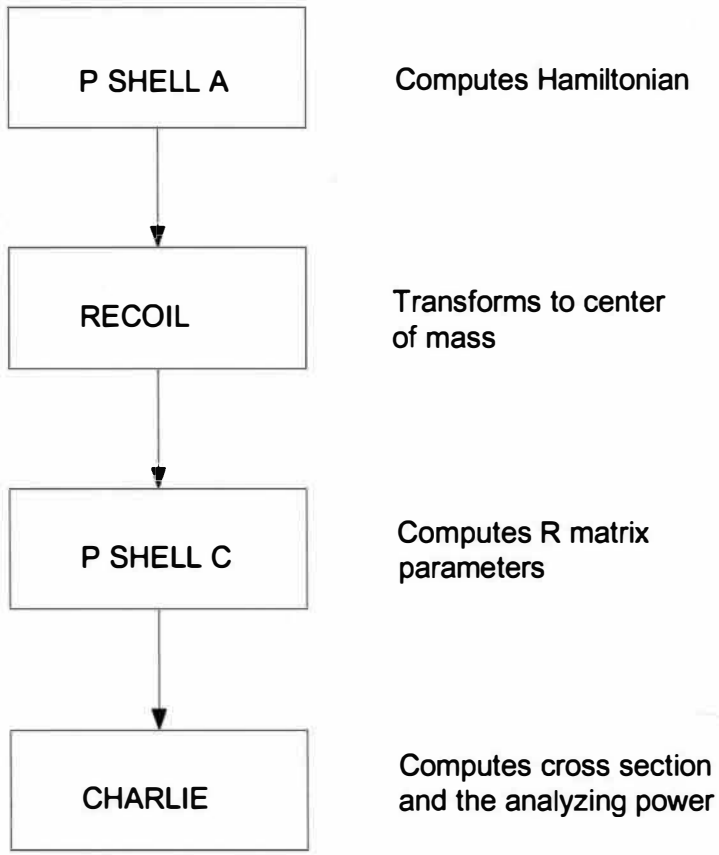

To use the RCCSM model, the first task is to solve the R-matrix equations. These equations can be written in the following form [5, 16]

$$\sum_{\lambda'=1}^{N}[<\lambda \mid H-E \mid \lambda'>+\sum_{c}\gamma_{\lambda c}(b_{\lambda' c}-b_c)\gamma_{\lambda' c}]A_{\lambda'}=0 \tag{10}$$

where b_c is the physical boundary condition parameter; $\gamma_{\lambda c}$ is the reduced widths and widths and $b_{\lambda c}$ is the logarithmic derivatives; and Hamiltonian H can be written as:

$$H=\sum_{i=1}^{A}\frac{p_i^2}{2m}-T_{c.m.}+\sum_{i<j}^{A}v_{ij}+\sum_{i<j<k}^{A}v_{ijk}' \tag{11}$$

The first step is to compute the Hamiltonian in equation (11), then go to the next step, to transform to the center-of-mass, where the matrix elements between α-states and β-states finally are transformed from the shell model coordinate, $\phi_{nl}(\mathbf{r}_0)$, to the coordinate of the center-of-mass, $\Psi_{\bar{n}\bar{l}}(\mathbf{r})$. The α-states are constructed by coupling the nonspurious shell model state of A-1 system to a single particle state to a good total angular momentum, and the β-states are the nonspurious shell model states of A system. The transformation equations refer to Fig. 2 and equations (12) - (15) are shown below:

$$_{\text{int}}<\beta J_B \parallel T^K \parallel \beta' J_B'>_{\text{int}}=_{SM}<\beta J_B \parallel T^K \parallel \beta' J_B'>_{SM} \tag{12}$$

$$_{\text{int}}<\alpha SnlJ_B \parallel T^K \parallel \beta' J_B'>_{\text{int}}=(1+A_c^{-1})^{\rho/2}{}_{SM}<\alpha SnlJ_B \parallel T^K \parallel \beta' J_B'>_{SM} \tag{13}$$

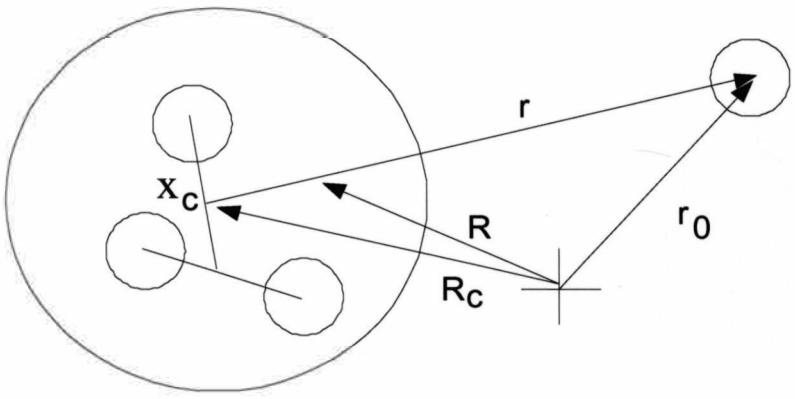

Figure 2: The RCCSM Coordinates. For the fixed origin, $\mathbf{R_c}$ locates the center-of-mass of core, $\mathbf{R}$ locates the center-of-mass of the composite system, $\mathbf{r_0}$ locates the

continuum nucleon; for the center-of-mass of the core, **r** locates the continuum nucleon.

$$_{\text{int}}<\alpha SnlJ_B \parallel T^k \parallel \alpha' S' n' l' J_B' >_{\text{int}} = (1+A_c^{-1})^{(\rho+\rho')/2}\{_{SM}<\alpha SnlJ_B \parallel T^K \parallel \alpha' S' n' l' J_B' >_{SM}$$

$$- \sum_{\bar{n}\bar{l}\bar{n}'\bar{l}'\bar{J}_B\bar{J}_B'} (coeff)_{\text{int}} <\alpha S \bar{n}\bar{l}\bar{J}_B \parallel T^K \parallel \alpha' S' \bar{n}'\bar{l}'\bar{J}_B'>_{\text{int}}\}, \qquad (14)$$

Where int means internal coordinates, SM means the shell model states, and

$$(coeff) = [\bar{J}_B]\hat{J}_B'\hat{\bar{J}}'_B\hat{\bar{l}}\hat{\bar{l}}' \sum_{NL\neq 00} W(S\bar{l}J_B L;\bar{J}_B l)W(S'\bar{l}'J_B' L;\bar{J}'_B l')W(\bar{J}_B kLJ_B';\bar{J}'_B;\bar{J}'_B J_B)$$

$$\times <\bar{n}\bar{l},NL,l \mid nl,00,l><\bar{n}'\bar{l}',NL,l'\mid n'l',00,l'> \qquad (15)$$

In equation (15), the angular brackets are the unequal mass Talmi-Moshinsky brackets, $[J]=2J+1$, $\hat{J}=(2J+1)^{1/2}$, $\rho=2n+l$, $A_0=A-1$ and the reduced matrix elements. Equation (14) is a recursion relation for the intrinsic matrix elements. Then the next step is to computer the R-matrix parameters, $\gamma_{\lambda c}$ and $b_{\lambda c}$ in equation (10). Finally, by using a FORTRAN program [18], the cross section and the analyzing power can be computed.

CHAPTER IV

RESULTS

In this chapter, all the theoretical curves are calculated based on the theory of chapter III. M3Y curve is calculated by using only the M3Y interaction; M3Y-MOD+Skyrme is calculated using M3Y interaction including Skyrme interaction, modified by fitting the energy spectra of ^{8}B and ^{8}Li and very low energy scattering data. The modifications of M3Y include multiplying, the spin-orbit function $V = \sum V_i Y(r_{12} / R_i) L \bullet S$ by 1.293, and tensor function $V = \sum V_i r_{12}^2 Y(r_{12} / R_i) S_{12}$ by 0.7. In addition, a Skyrme interaction of strength $t_3 = 1810\ MeVfm^6$ is included. M3Y+Skyrme curve is calculated with the unmodified M3Y interaction and Skyrme interaction with strength t_3 in $1810\ MeVfm^6$.

Elastic Scattering of ^{6}Li and ^{7}Li

The elastic scattering differential cross section σ and the analyzing power A_y data about ^{6}Li with proton energy $E_p = 49.75\ MeV$ are shown in Fig. 3 and Fig. 4. This calculation include the core states $^{6}Li(1^+, 0^+, and\, 3^+)$ and $^{6}He(0^+)$.

In the differential cross section plot, the circle dot points are the experiment data; the red line is the theoretical calculation with the M3Y interaction plus Skyrme interaction with $t_3 = 1810\ MeVfm^6$; the dash dot line is theoretical calculation which uses only the M3Y interaction, and the dot line is using M3Y-MOD+SKYRME. The theoretical results of ^{6}Li for the differential cross section in different effective forces give a good agreement with the experimental cross section for $\theta < 150^0$ shown in Fig. 5. One sees that the addition of a Skyrme component gives a more diffractive cross

section; M3Y-MOD+SKYRME gives the best agreement of the three interactions. However, the calculated analyzing power is too small at 80^0 and does not dip negative at 130^0. This problem is not solved by the increased spin orbit force in M3Y-MOD+SKYRME or by adding a Skyrme component. One notes that the differential cross section will not change much by adding the Skyrme interaction. The analyzing power is more sensitive than the differential cross section, but the changes are still small. This is because, for the Skyrme interaction in ^{6}Li, one has only $\binom{7}{3} = 35$ three-body interactions. One expects a larger effect in the A=8 system where the Skyrme interaction has $\binom{8}{3} = 56$ three-body interactions.

For the A = 8 systems, the core states in conclude are $^7Li(3/2^-,1/2^-,7/2^-)$ and $^7Be(3/2^-,1/2^-,7/2^-)$. The elastic scattering differential cross section and the analyzing power data for $^7Li + p$ at the proton energy $E_p = 49.75\ MeV$ are shown in Fig. 5 and Fig. 6. Although providing better agreement with the cross section data for $\theta < 110^0$, adding the Skyrme component causes a rise at back angles which is not observed in the data. The Skyrme component seems to be behaving like a repulsive core. The analyzing power does seem to improve with the addition of the Skyrme component; however, it is unfortunate that the analyzing power data does not extend beyond 90^0 where large differences in the calculation occur.

Charge Exchange Reactions

Cross sections for the reaction $^7Li(p,n)^7Be$ are shown in Fig. 7 and Fig. 8 at proton energies of $18.9\ MeV$ and $26\ MeV$. One sees that what agreement with the data was provided by M3Y becomes less when the Skyrme component is added. The cross section with Skyrme becomes severely diffractive.

The $^7Li(p,n)^7Be$ and $^7Li(p,n)^7Be^*(1/2^-)$ cross sections at $E_p = 45$

MeV are shown in Fig. 9 and Fig. 10. The effect of adding the Skyrme interaction is much less. In fact, M3Y-MOD+SKYRME seems to give the best agreement with the data.

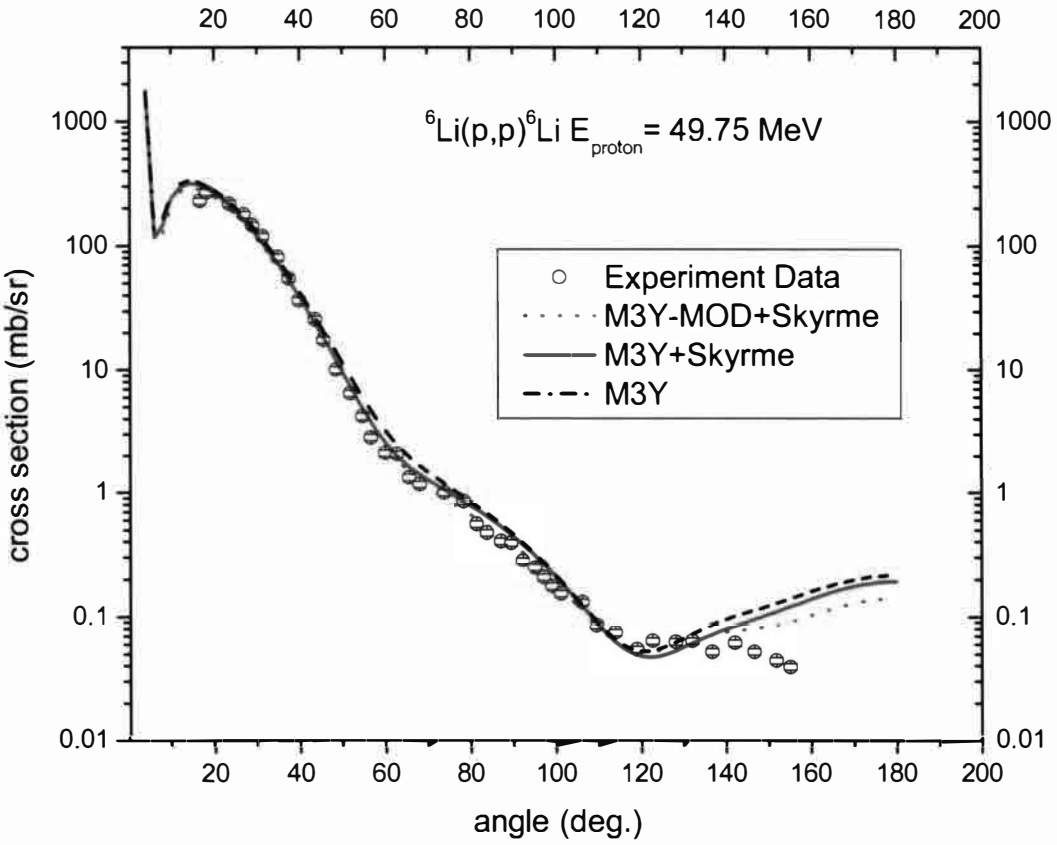

Figure 3: Scheme of ^{6}Li Differential Cross Section in Theoretical Calculation and of the Experimental Data Points for Proton Energy 49.75 *MeV*. The circle dot points are the experimental data points from reference [19, 20], the lines are the theoretical calculations in different effective interactions shown as in the figure.

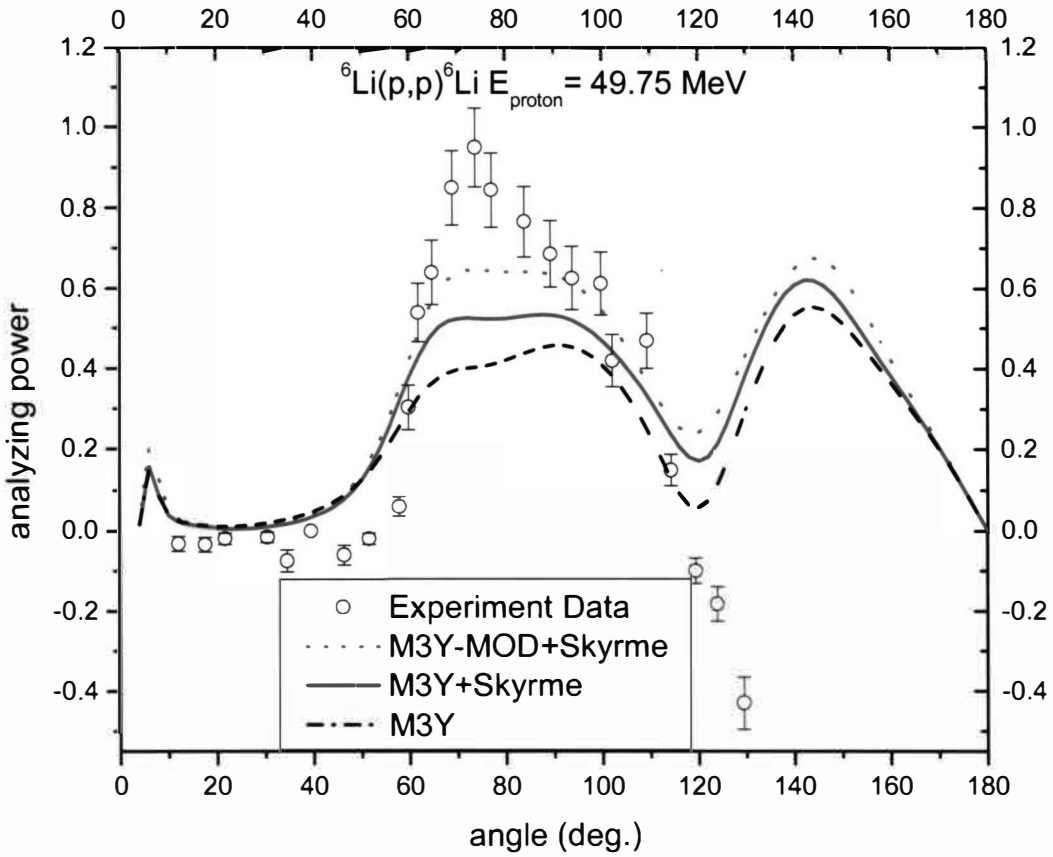

Figure 4: Scheme of ^{6}Li Analyzing Powers in Theoretical Calculation and of the Experimental Data Points for Proton Energy 49.75 *MeV* . The circle dot points are the experimental data points from reference [19, 20], and the lines are the theoretical calculations in different effective interactions shown as in the figure.

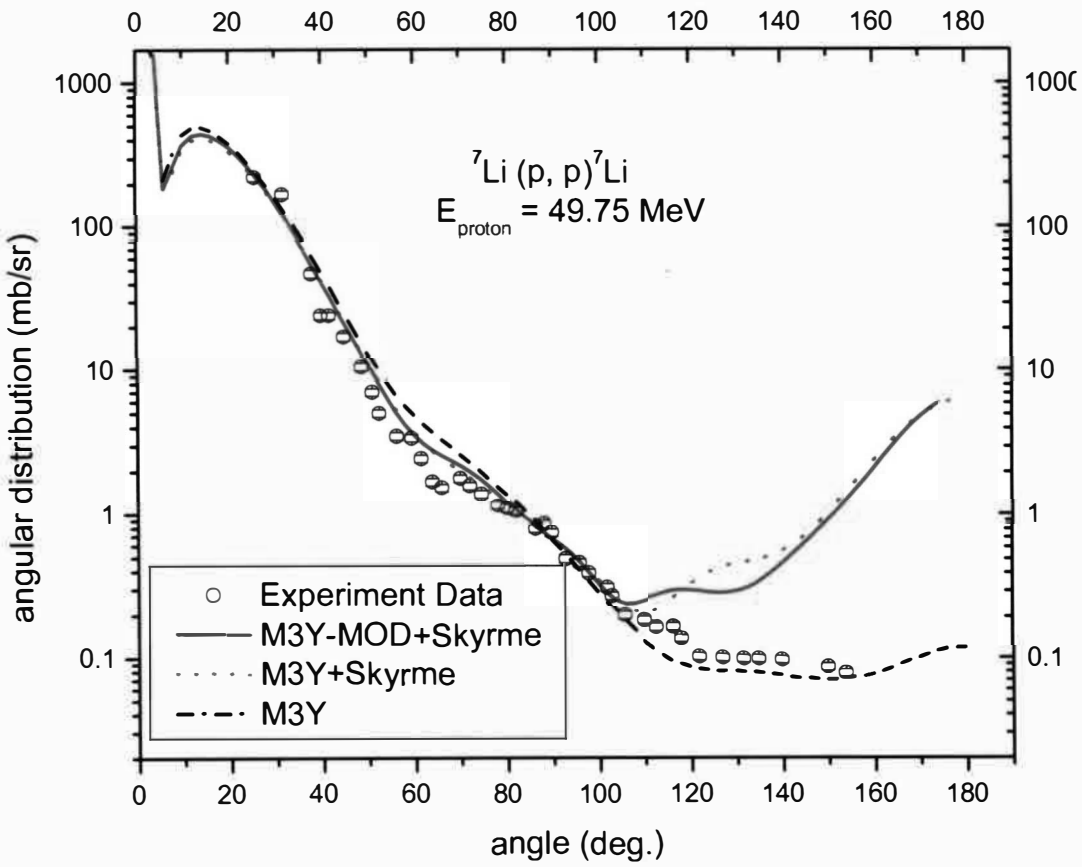

Figure 5: Scheme of ^{7}Li Differential Cross Section in Theoretical Calculation and of the Experimental Data Points for Proton Energy 49.75 *MeV* . The experimental data is from reference [20], circle dot points are the experimental data points, the lines are the theoretical calculations in different effective interactions shown as in the figure.

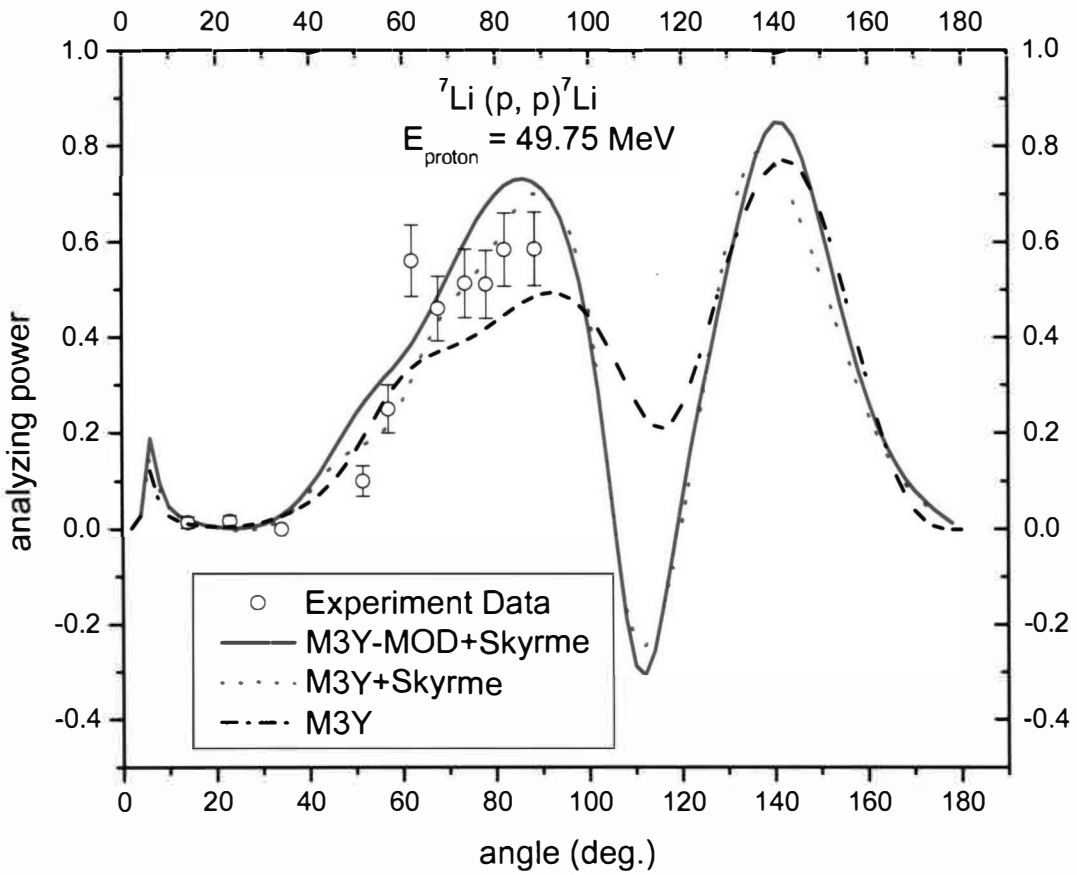

Figure 6: Scheme of ^{7}Li Analyzing Powers in Theoretical Calculation and of the Experimental Data Points for Proton Energy 49.75 *MeV* . The experimental data is from reference [20], circle dot points are the experimental data points, the lines are the theoretical calculations in different effective interactions shown as in the figure.

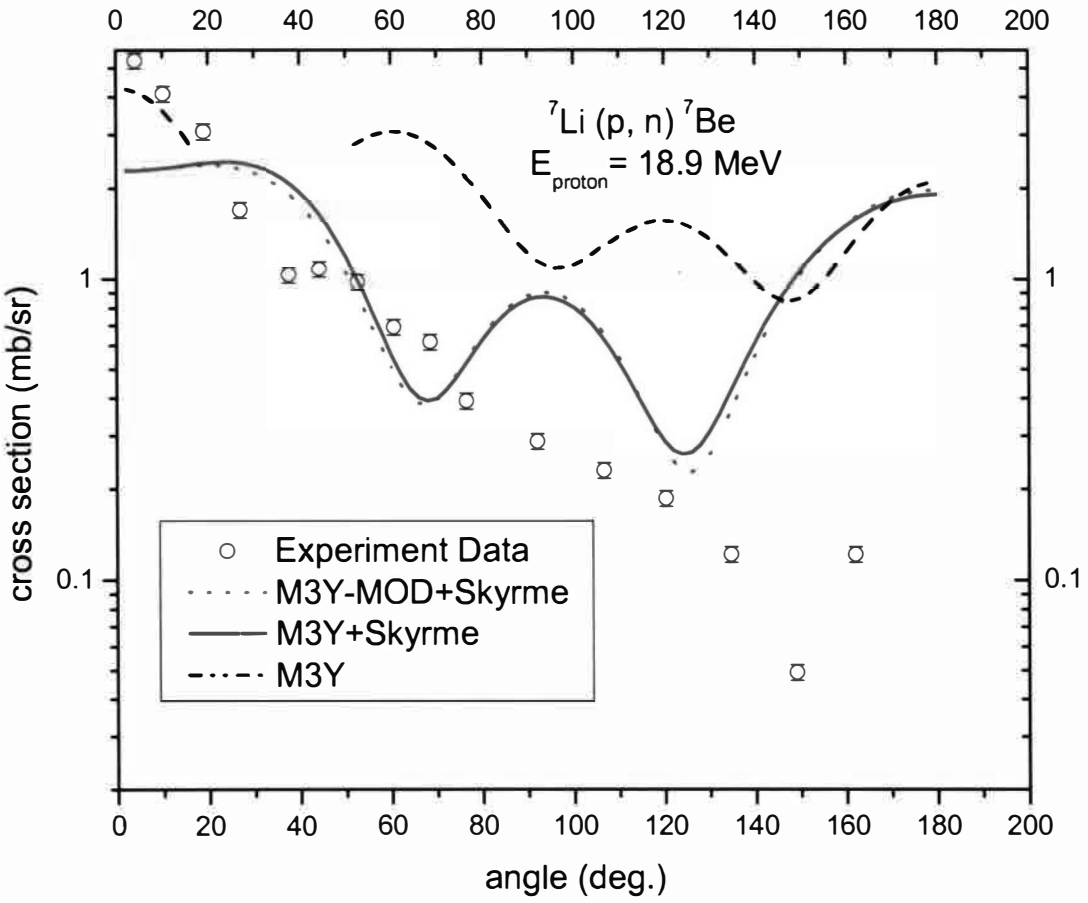

Figure 7: Scheme of Differential Cross Section in Theoretical Calculation and of the Experimental Data Points for Proton Energy 18.9 *MeV* . The circle dot points are the experimental data points from reference [21], the lines are the theoretical calculations in different effective interactions shown as in the figure.

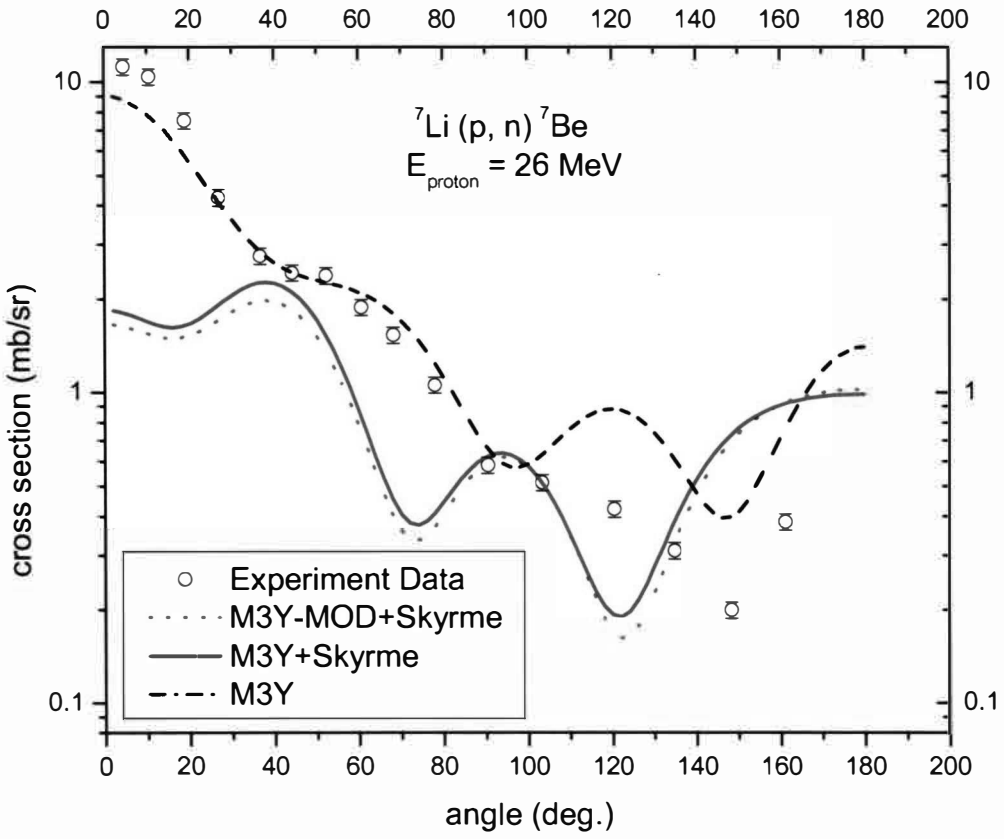

Figure 8: Scheme of Differential Cross Section in Theoretical Calculation and of the Experimental Data Points for Proton Energy 26 *MeV* . The circle dot points are the experimental data points from reference [21], the lines are the theoretical calculations in different effective interactions shown as in the figure.

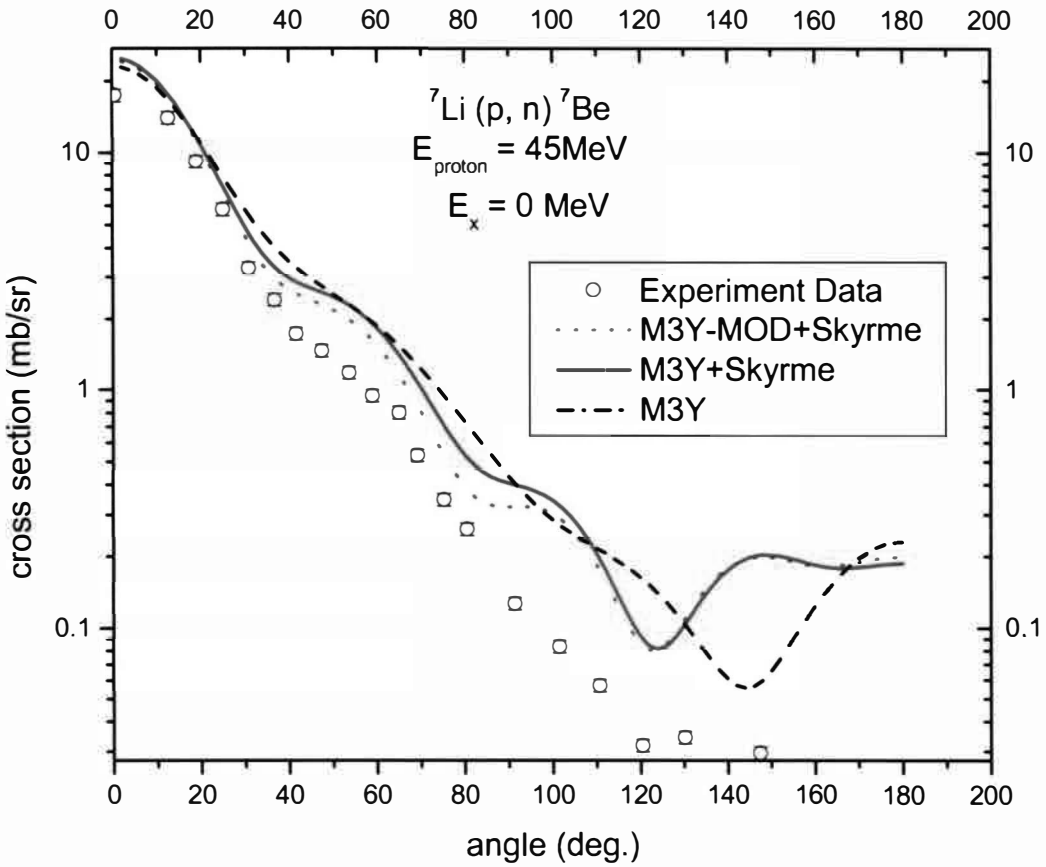

Figure 9: Scheme of Differential Cross Section in Theoretical Calculation and of the Experimental Data Points for Proton Energy 45 MeV and $E_x = 0\ MeV$. The circle dot points are the experimental data points from reference [22], the lines are the theoretical calculations in different effective interactions shown as in the figure.

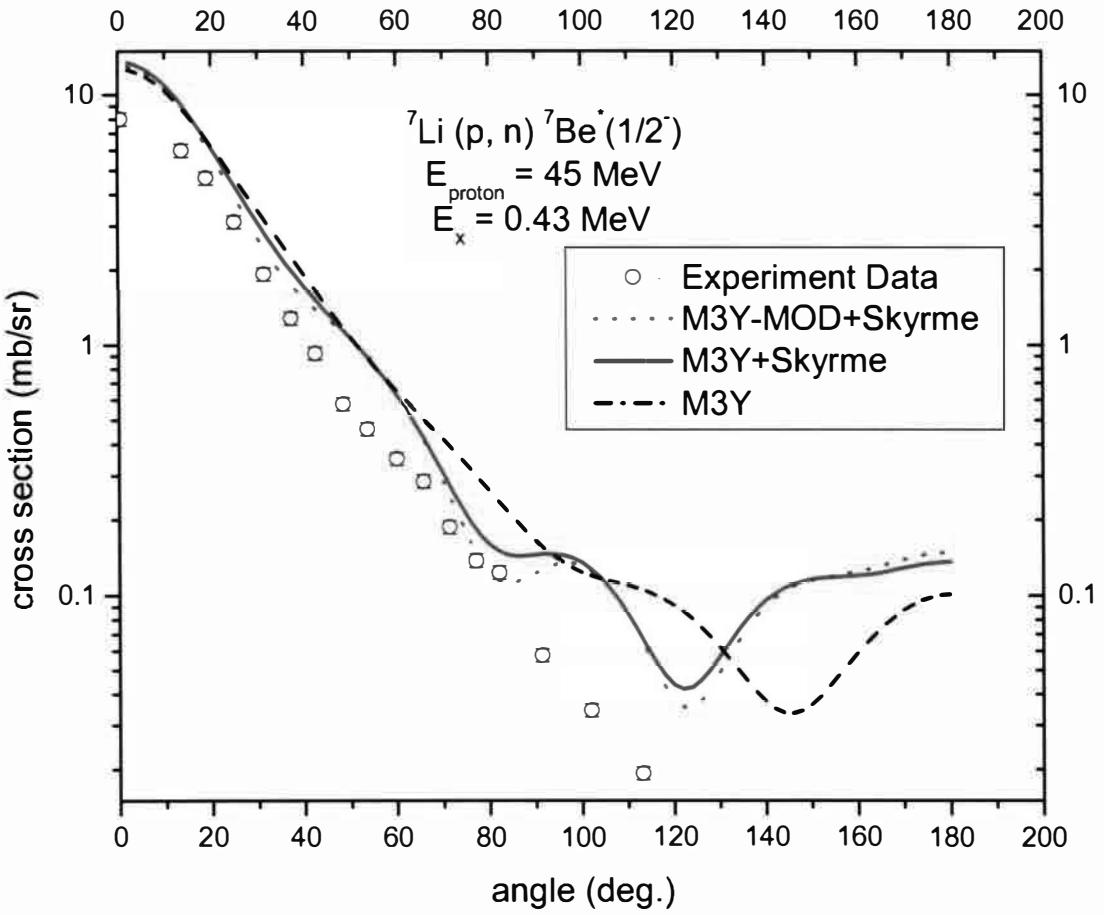

Figure 10: Scheme of Differential Cross Section in Theoretical Calculation and of the Experimental Data Points for Proton Energy 45 MeV and $E_x = 0.43\ MeV$. The circle dot points are the experimental data points from reference [22], the lines are the theoretical calculations in different effective interactions shown as in the figure.

Inelastic Scattering from Li^7

The inelastic scattering differential cross section ^{7}Li with proton energy $E_p = 24.4\ MeV$ exciting the $1/2^-$ state (in Fig. 11) at $E_x = 0.48\ MeV$ and the $7/2^-$ state (in Fig. 11) at $E_x = 4.63\ MeV$ are shown in Fig. 12 and Fig. 13. Proton energy $E_p = 49.8\ MeV$ under $E_x = 0.48\ MeV$ and $E_x = 4.63\ MeV$ are shown in Fig. 14 and Fig. 15.

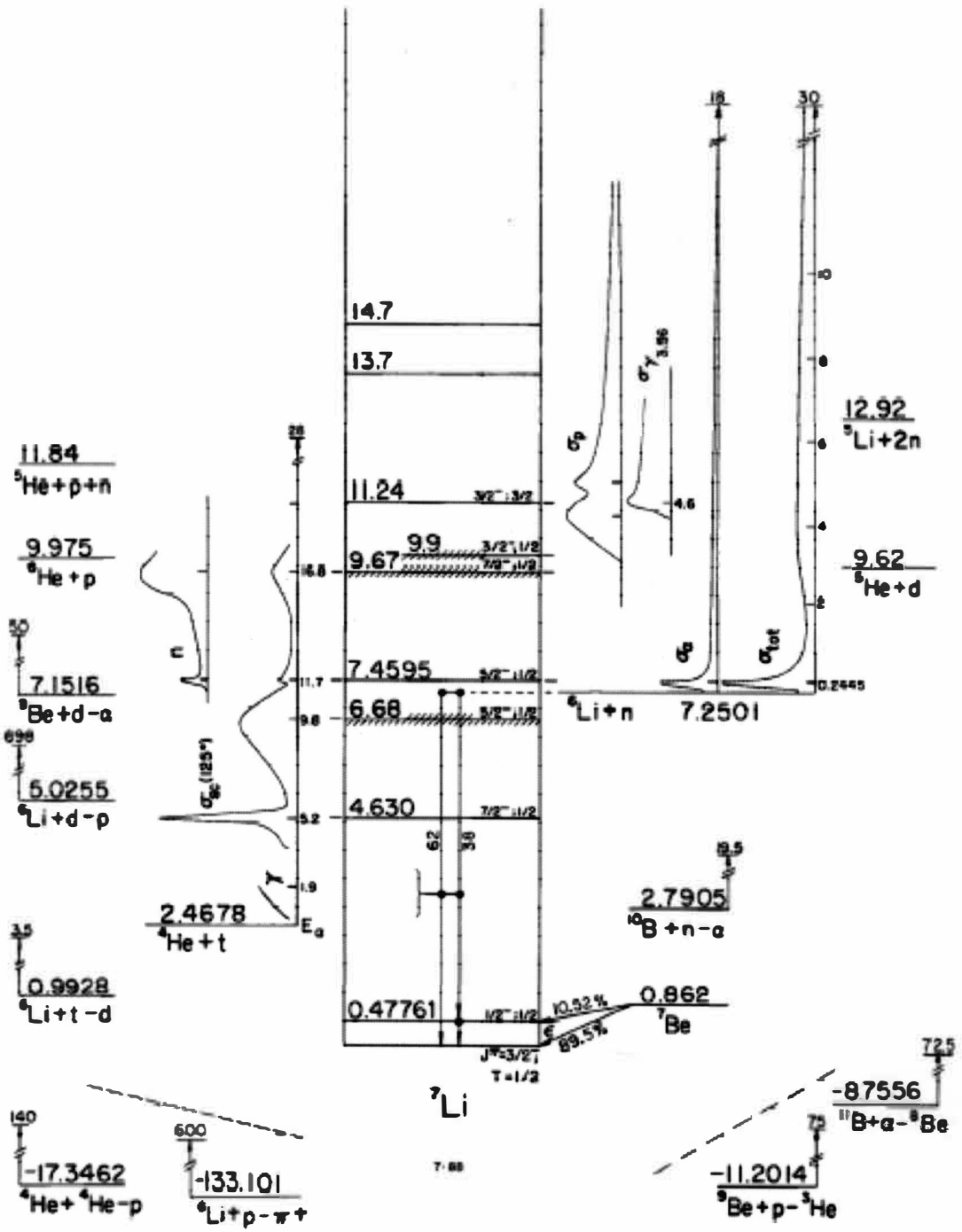

Figure 11: Scheme of Energy Level Diagram of ^{7}Li. This is from reference [23].

For $E_p = 24.4\ MeV$, the results are reminiscent of the low energy (p,n) cross sections. The addition of the Skyrme interaction gives much worse agreement with the data as compared to M3Y interaction only. However, for $E_p = 49.8\ MeV$ with $E_x = 0.48\ MeV$ in Fig. 14, one sees good agreement with the data for all three interactions. While for $E_p = 49.8\ MeV$ with $E_x = 4.63\ MeV$ in Fig. 15, the red line and the dot line fit better than the dash dot line which uses only the M3Y interaction.

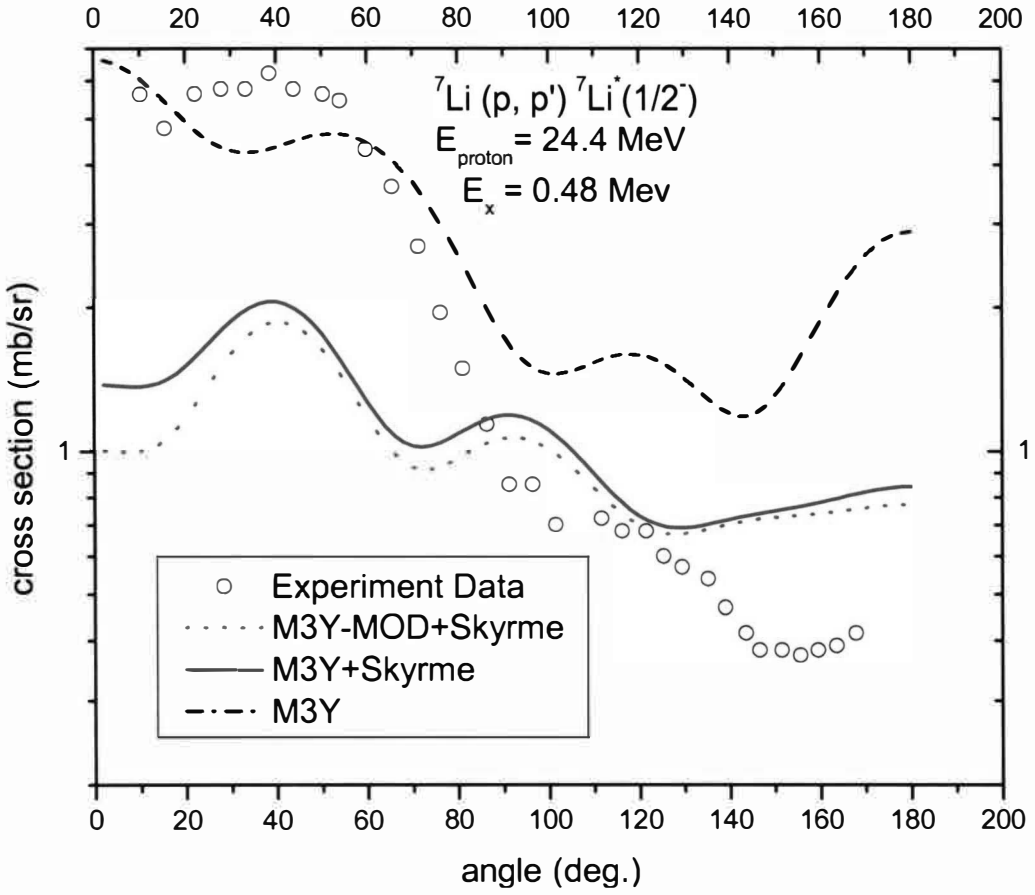

Figure 12: Scheme of Differential Cross Section in Theoretical Calculation and of the Experimental Data Points for Proton Energy 24.4 MeV and $E_x = 0.48\ MeV$. The circle dot points are the experimental data points from reference [22], the lines are the theoretical calculations in different effective interactions shown as in the figure.

The trend is now clear. By comparing with the different proton energies in Fig. 12 and Fig. 13, Fig. 14 and Fig. 15, at the higher proton energies, one improves the agreement with the data by adding the Skyrme interaction, but destroys the agreement at the lower energies. The modifications to M3Y in M3Y-MOD+SKYRME also improve agreement at higher energies.

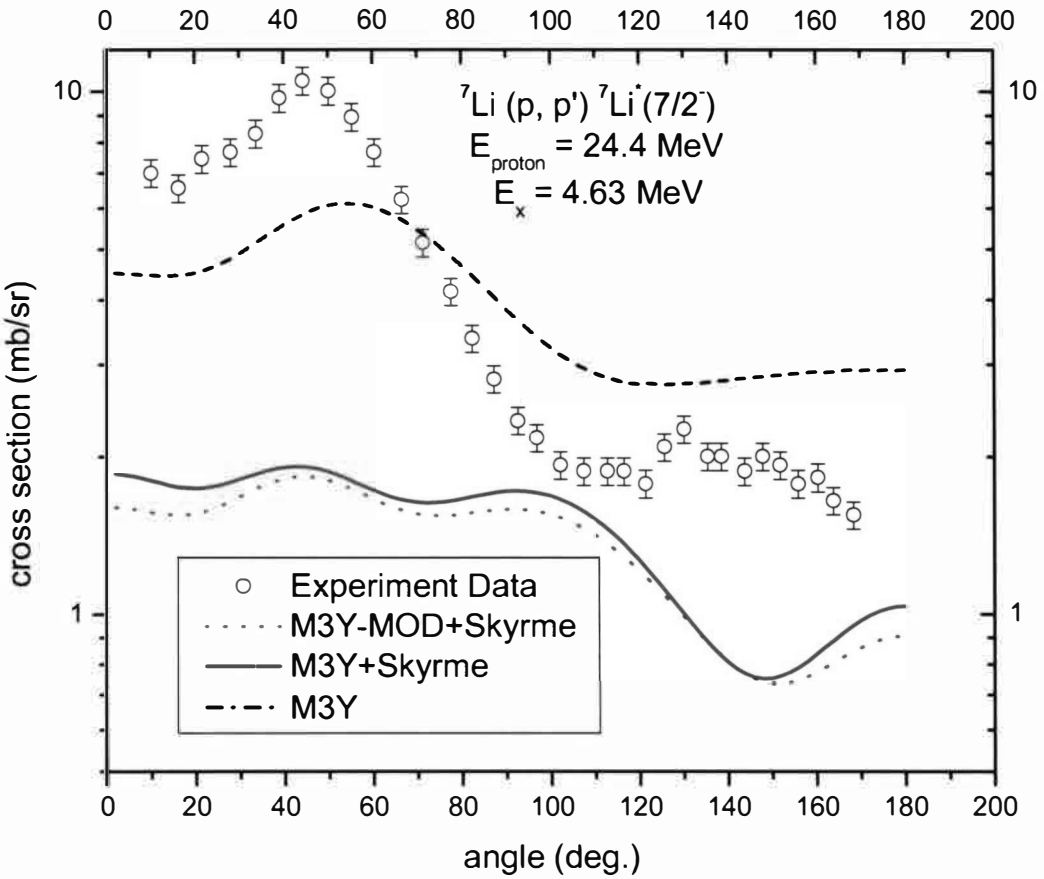

Figure 13: Scheme of Differential Cross Section in Theoretical Calculation and of the Experimental Data Points for Proton Energy 24.4 MeV and $E_x = 4.63\ MeV$. The circle dot points are the experimental data points from reference [22], the lines are the theoretical calculations in different effective interactions shown as in the figure.

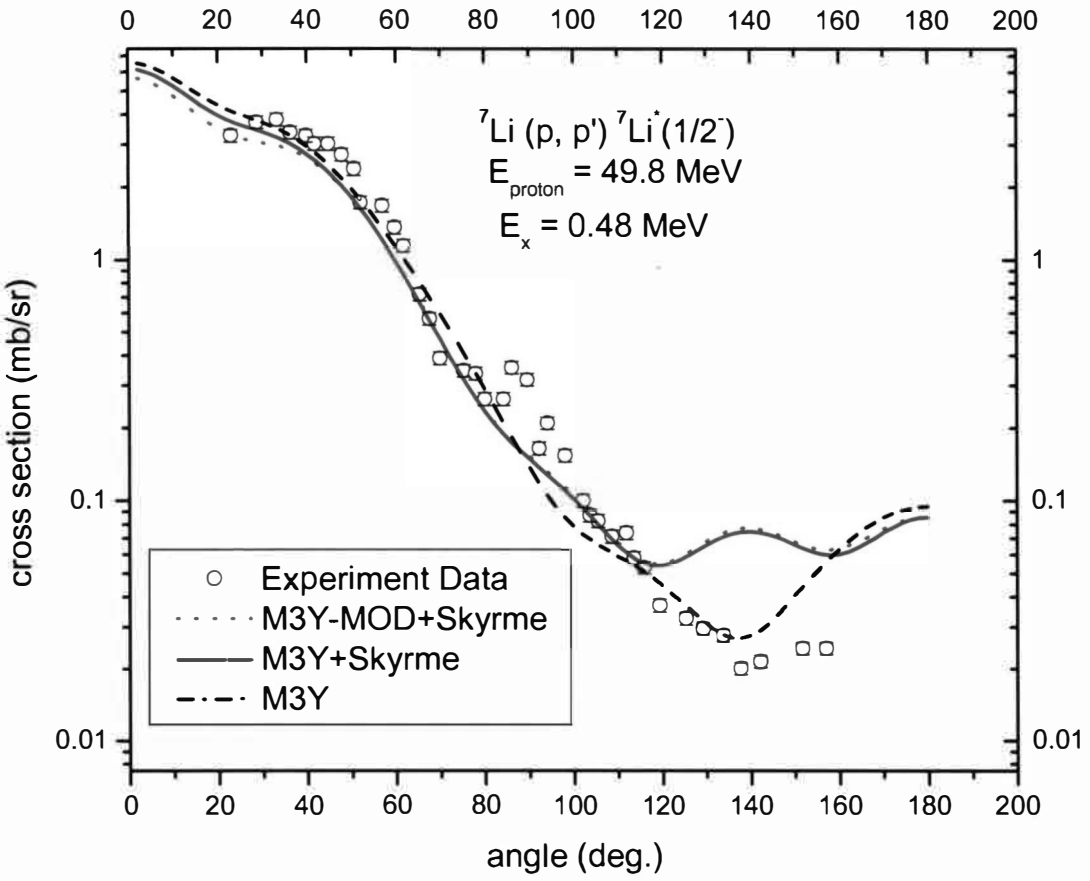

Figure 14: Scheme of Differential Cross Section in Theoretical Calculation and of the Experimental Data Points for Proton Energy 49.8 MeV and $E_x = 0.48\ MeV$. The circle dot points are the experimental data points from reference [22], the lines are the theoretical calculations in different effective interactions shown as in the figure.

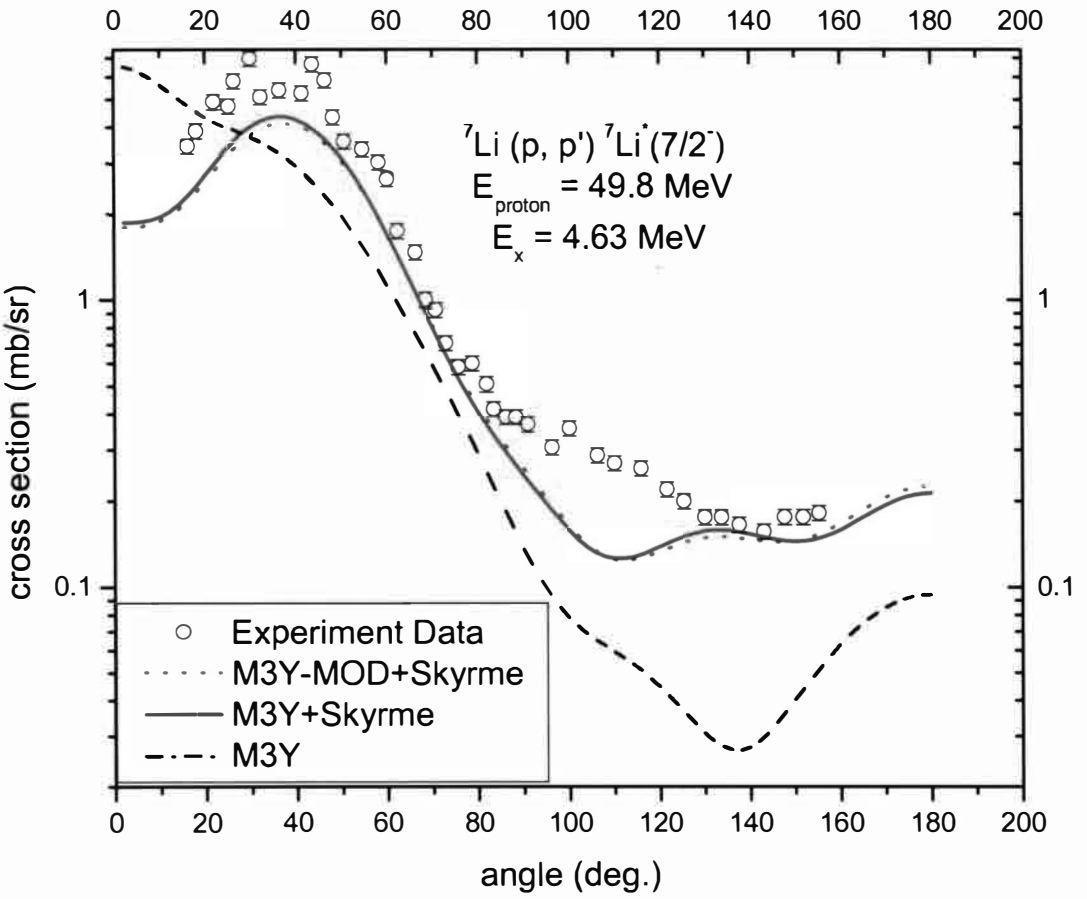

Figure 15: Scheme of Differential Cross Section in Theoretical Calculation and of the Experimental Data Points for Proton Energy 49.8 MeV and $E_x = 4.63\ MeV$. The circle dot points are the experimental data points from reference [22], the lines are the theoretical calculations in different effective interactions shown as in the figure.

Elastic Scattering of Proton from ^{14}N

Our example from the end of the p-shell has been calculated. The elastic scattering differential cross section about ^{14}N with proton energy $E_p = 31.0\ MeV$ are shown in Fig. 16. Calculations are made for M3Y, M3Y + Skyrme, M3Y + 2 × Skyrme, M3Y + 3 × Skyrme, and M3Y + 4 × Skyrme. The oscillator size parameter employed is $\nu = m\varpi/\hbar = 0.33 fm^{-1}$. The back-angle rise seen in Fig. 5 for ^{7}Li is

eliminated by including all ^{14}N and ^{14}O core states. This acts like adding absorption in an optical model. One can see that with increasing the Skyrme interaction, the cross section becomes more diffractive, like the data. For four times Skyrme interaction, the calculation looks reasonable, and a good fit for $\theta < 90^0$ could be obtained by increasingv. The value of $t_3 = 7240\ MeVfm^6$ is very close to the $8000\ MeVfm^6$ used in Skyrme's original article. Wave functions from calculations such as this would be very useful in knockout reactions.

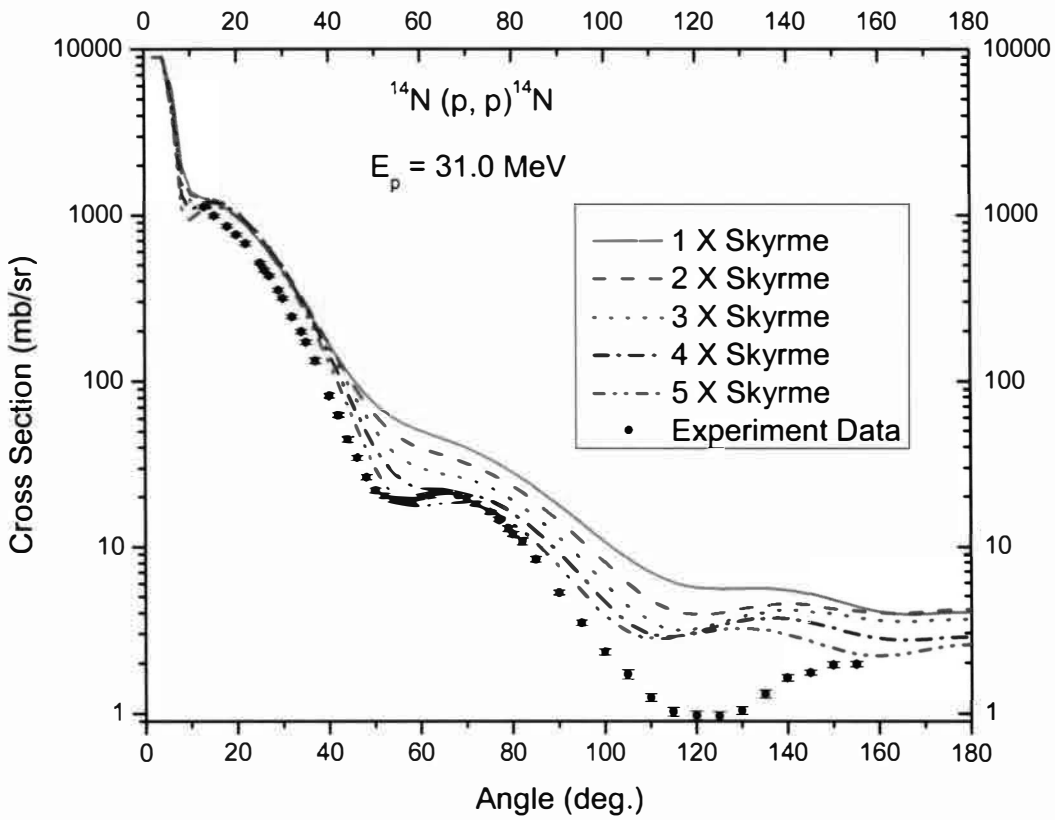

Figure 16: Differential Elastic Scattering Cross Section of ^{14}N with Different Skyrme Interaction for $E_p = 31.0\ MeV$. Solid line represents the adding Skyrme interaction. Dashes represent twice Skyrme interaction. Dots represent three times Skyrme interaction. Dash Dots represent four times Skyrme interaction. Dash Dot Dot represents five times Skyrme interaction. Circle points represent experimental data from reference [24].

CHAPTER V

CONCLUSIONS

This thesis has described the results for three different effective interactions for nucleon scattering on light nuclei. The RCCSM was employed to calculate the cross section and the analyzing power. Target nuclei included ^{7}Li, ^{6}Li and ^{14}N. The RCCSM model was employed because it eliminates spurious center-of-mass excitations and uses realistic effective interactions.

The results, given the three theoretical models employed, show that the M3Y interaction with the Skyrme interaction added is in agreement with the experimental result for the higher proton energies. The Skyrme interaction plus modifications to M3Y did even better. However, for lower proton energy, the inclusion of a Skyrme component destroyed with the experimental data.

It is difficult to analyze a RCCSM calculation. One cannot divide the calculation up into a form factor and incident and exit optical potentials as one would do in a DWA calculation. However, the original form of the Skyrme interaction used in this work has a very simple form. It was no spin or isospin dependence. Adding the spin or isospin term in Skyrme interaction three-body term will be the future work.

APPENDIX A

TABLE OF BEST FIT INTERACTIONS

Table 1. Best Fit Interactions

Label	Channel	Name	V_t		
			R_1=0.25	R_2=0.40	R_3=max
1	SE	Reid	12454	-3835	-10.463
2	TE	Reid	21227	-6622	-10.463
3	TNE	Reid	0.0	-1259.6	-18.41
4	TNO	Elliott	0.0	283	13.62
5	LSE	Elliott	0.0	-813	0.0
6	LSO	Reid	-3733	-427.3	0.0
7	SO	ALTSO	5018	1810	0.0

APPENDIX B

CLEBSH-GORDEN COEFFICIENTS DERIVATION

The six terms in equations (3) to (9) may be reduced to the following expressions, Equations (4) and (7) are in the form

$$< i >= P_1 I_1 [J]^{-1} \{1/2 C_1 (S_1 C_2 + S_2 C_3) + C_4 S_3\}$$

Where for <1>:

$$C_1 = C(j_2' j_3' J_{23}' \tfrac{1}{2}, 1),$$

$$C_1 = C(j_2' j_3' J_{23}' \tfrac{1}{2}, 1),$$

$$C_2 = (-1)^{J_{23}'+J_{23}+1} C(J_{23}' j_1' J 1 \tfrac{1}{2} \tfrac{3}{2}),$$

$$C_3 = (-1)^{l_1+l_1'+1} C(J_{23}' j_1' J -1 \tfrac{1}{2} -\tfrac{1}{2}), \quad P_1 = (-1)^{J_{23}+j_2'-j_3'}, \text{ and}$$

$$C_4 = \tfrac{1}{2}[1 + (-1)^{l_1+l_1'+J_{23}+J_{23}'}](-1)^{l_2+l_2'+J_{23}+J_{23}'+j_2+j_2'} C(j_2' j_3' J_{23}' -\tfrac{1}{2} \tfrac{1}{2} 0) C(J_{23}' j_1' J 0 \tfrac{1}{2} \tfrac{1}{2}).$$

For <4>:

$$C_1 = C(j_3' j_2' J_{23}' \tfrac{1}{2} \tfrac{1}{2}, 1),$$

$$C_2 = (-1)^{J_{23}'+J_{23}+1} C(J_{23}' j_1' J 1 \tfrac{1}{2} \tfrac{3}{2}),$$

$$C_3 = (-1)^{l_1+l_1'+1} C(J_{23}' j_1' J -1 \tfrac{1}{2} -\tfrac{1}{2}), \quad P_1 = (-1)^{J_{23}+J_{23}'+1}, \text{ and}$$

$$C_4 = \tfrac{1}{2}[1 + (-1)^{l_1+l_1'+J_{23}+J_{23}'}](-1)^{l_2+l_3'+J_{23}+J_{23}'+j_2+j_3'} C(j_3' j_2' J_{23}' -\tfrac{1}{2} \tfrac{1}{2} 0) C(J_{23}' j_1' J 0 \tfrac{1}{2} \tfrac{1}{2}).$$

Equations (5)-(9) are in the form:

$$< i >= \tfrac{1}{2} P_1 I_1 \hat{J}^{-1} \hat{J}'^{-1}_{23} \{\tfrac{1}{2}(S_1 C_1 + S_2 C_2 + P_2 S_3 (C_3 + C_4))\},$$

Where for <2>:

$$C_1 = (-1)^{J_{23}'+J_{23}+j_3'+1/2} C(j_1' J J_{23}' \tfrac{1}{2} -\tfrac{3}{2} -1), \quad C(j_3' j_2' J_{23}' \tfrac{1}{2} \tfrac{1}{2} 1),$$

$$C_2 = (-1)^{l_1+l_3'+J+J_{23}'+1/2} C(j_1' J J_{23}' \tfrac{1}{2} -\tfrac{1}{2} 0), C(j_3' j_2' J_{23}' -\tfrac{1}{2} \tfrac{1}{2} 1), \text{ and}$$

$$P_2 = (-1)^{l_2+l_2'+j_2+J_{23}+j_2'},$$

$$C_3 = (-1)^{j_3'+J_{23}'-1/2} C(j_1' J J_{23}' \tfrac{1}{2} -\tfrac{1}{2} 0), \quad C(j_3' j_2' J_{23}' -\tfrac{1}{2} \tfrac{1}{2} 1), \text{ and}$$

$$P_1 = (-1)^{J-J_{23}-j_3+1},$$
$$C_4 = (-1)^{l_2+l_3'-J_{23}+J_{23}'+J-1/2} C(j_3' j_2' J_{23}' -\tfrac{1}{2} -\tfrac{1}{2} -1) C(j_1' J J_{23}' \tfrac{1}{2} \tfrac{1}{2} 1).$$

For <3>:

$$C_1 = (-1)^{J_{23}'+J_{23}+J-1/2} C(j_1' J J_{23}' -\tfrac{1}{2} \tfrac{3}{2} 1),\ C(j_2' j_3' J_{23}' -\tfrac{1}{2} -\tfrac{1}{2} -1),$$
$$C_2 = (-1)^{l_1+l_2'+j_2'+J_{23}'-1/2} C(j_1' J J_{23}' \tfrac{1}{2} -\tfrac{1}{2} 0),\ C(j_2' j_3' J_{23}' \tfrac{1}{2} -\tfrac{1}{2} 0), \text{ and}$$

$$P_2 = (-1)^{l_2+l_1'+j_2+J_{23}+j_1'},$$
$$C_3 = (-1)^{J+J_{23}'-1/2} C(j_1' J J_{23}' \tfrac{1}{2} -\tfrac{1}{2} 0),\ C(j_2' j_3' J_{23}' -\tfrac{1}{2} \tfrac{1}{2} 1), \text{ and}$$

$$P_1 = (-1)^{J-J_{23}+J_{23}'+j_1'},$$
$$C_4 = (-1)^{l_1+l_2'-J_{23}+J_{23}'+j_2'-1/2} C(j_2' j_3' J_{23}' \tfrac{1}{2} -\tfrac{1}{2} 0) C(j_1' J J_{23}' \tfrac{1}{2} -\tfrac{1}{2} 0).$$

For <5>:

$$C_1 = (-1)^{J_{23}'+J_{23}+J-1/2} C(j_1' J J_{23}' -\tfrac{1}{2} \tfrac{3}{2} 1),\ C(j_3' j_2' J_{23}' -\tfrac{1}{2} -\tfrac{1}{2} -1),$$
$$C_2 = (-1)^{l_1+l_3'+j_3'+J_{23}'-1/2} C(j_1' J J_{23}' -\tfrac{1}{2} \tfrac{1}{2} 0),\ C(j_3' j_2' J_{23}' \tfrac{1}{2} -\tfrac{1}{2} 0), \text{ and}$$

$$P_2 = (-1)^{l_2+l_1'+j_2+J_{23}+j_1'},$$
$$C_3 = (-1)^{J+J_{23}'-1/2} C(j_1' J J_{23}' \tfrac{1}{2} \tfrac{1}{2} 1),\ C(j_3' j_2' J_{23}' -\tfrac{1}{2} -\tfrac{1}{2} -1), \text{ and}$$

$$P_1 = (-1)^{J-J_{23}+j_1'+j_2'+j_3'},$$
$$C_4 = (-1)^{l_1+l_3'-J_{23}+J_{23}'+j_3'-1/2} C(j_3' j_2' J_{23}' \tfrac{1}{2} -\tfrac{1}{2} 0) C(j_1' J J_{23}' \tfrac{1}{2} -\tfrac{1}{2} 0).$$

For <6>:

$$C_1 = (-1)^{J_{23}'+J_{23}+j_2'+1/2} C(j_1' J J_{23}' \tfrac{1}{2} -\tfrac{3}{2} -1),\ C(j_2' j_3' J_{23}' \tfrac{1}{2} \tfrac{1}{2} 1),$$
$$C_2 = (-1)^{l_1+l_2'+J+J_{23}'+1/2} C(j_1' J J_{23}' \tfrac{1}{2} -\tfrac{1}{2} 0),\ C(j_2' j_3' J_{23}' -\tfrac{1}{2} \tfrac{1}{2} 0), \text{ and}$$

$$P_2 = (-1)^{l_2+l_3'+j_2+J_{23}+j_3'},$$
$$C_3 = (-1)^{j_2'+J_{23}'-1/2} C(j_1' J J_{23}' \tfrac{1}{2} -\tfrac{1}{2} 0),\ C(j_2' j_3' J_{23}' \tfrac{1}{2} -\tfrac{1}{2} 0), \text{ and}$$

$$P_1 = (-1)^{J-J_{23}+J_{23}'+j_3'},$$
$$C_4 = (-1)^{l_1+l_2'-J_{23}+J_{23}'+J-1/2} C(j_2' j_3' J_{23}' -\tfrac{1}{2} -\tfrac{1}{2} -1) C(j_1' J J_{23}' \tfrac{1}{2} \tfrac{1}{2} 1).$$

In the above equations:

$$S_1 = C(j_2 j_3 J_{23} -\tfrac{1}{2} -\tfrac{1}{2} -1) C(j_1 J_{23} J -\tfrac{1}{2} -1 -\tfrac{3}{2}).$$

$$S_2 = C(j_2 j_3 J_{23} - \tfrac{1}{2} - \tfrac{1}{2} - 1) C(j_1 J_{23} J - \tfrac{1}{2} 1 \tfrac{1}{2})$$

$$S_3 = C(j_2 j_3 J_{23} \tfrac{1}{2} - \tfrac{1}{2} 0) C(j_1 J_{23} J - \tfrac{1}{2} 1 \tfrac{1}{2})$$

$$[j] = 2j + 1$$

$I_1 = \hat{j}_1 \hat{j}_2 \hat{j}_3 \hat{j}_1' \hat{j}_2' \hat{j}_3' \int_0^\infty R_1^+ R_2^+ R_3^+ R_1 R_2 R_3 r^2 dr / (32\pi^2)$, and $\hat{j} = \sqrt{2j+1}$.

The above expressions also require the Kronecker deltas equations (5) through (9).

REFERENCES

[1] G.Bertsch, J. Borysowicz and H. Mcmanus and W. G. Love, Nucl. Phys. A **284**, 399 (1977)

[2] D. Halderson, Nucl. Phys. A **707**, 65 (2002)

[3] T. H. Skyrme, Nucl. Phys. **9**, 615 (1959)

[4] R. J. Philpott, Nucl. Phys. A **289**, 109 (1977)

[5] D. Halderson, International J. of Mod. Phys. E. **14**, 171 (2005)

[6] D. Halderson and R. J. Philpott, Nucl. Phys. A **321**, 295 (1979)

[7] D. Halderson and V. A. Sadovnikova, Phys. Rev. C **56**, 2688 (1997)

[8] D. Halderson, J. Phys. G **20**, 1461 (1994)

[9] T. Hamada and I. D. Johnston, Nucl. Phys. **34**, 382 (1962)

[10] R. Reid, Ann. Of Phys. **50**, 411 (1968)

[11] J. P. Elliott et al., Nucl. Phys. A **121**, 241 (1968)

[12] D. Vautherin and D. M. Brink, Phys. Rev. C **5**, 626 (1972)

[13] U. Fano, Phys. Rev. **124**, 1866 (1961)

[14] C. Block, *Many-Body Description of Nuclear Structure and Reactions*, Proc. Int. School of Phys. "Enrico Fermi" Course XXXVI, ed. C. Block (Academic Press, Inc., New York, 1966), p. 394

[15] R. J. Philpott, Fizika **9**, (Suppl.) 3, 21 (1977)

[16] R. J. Philpott, Nucl. Phys. A **243**, 260 (1975)

[17] A. M. Lane and R. G. Thomas, Rev. Mod. Phys. **30**, 257 (1958)

[18] "Fortran Program" written by Charlie, and R. J. Philpott

[19] G. S. Mani, D. Jacques, A. D. B. Dix, Nucl. Phys. A **165** 145 (1971)

[20] G. S. Mani, D. Jacques, A. D. B. Dix, Nucl. Phys. A **172** 166 (1971)

[21] C. H. Poppe, J. D. Anderson, J. C. Davis, S. M. Grimes, and C. Wong, Phys. Rev. C **14**, 438 (1976)

[22] F. Petrovich, R. H. Howell, C. H. Poppe, S. M. Austin and G. M. Crawley, Nucl. Phys. A **383** 355 (1981)

[23] TUNL Nuclear Data Evaluation website

[24] C. C. Kim, S. M. Bunch, D. W. Devins and H. H. Forster, Nucl. Phys. **58**, 32 (1964)